Mineralogical Magazine, February 2015, Vol. 79(1), pp. 1–10

In situ Raman spectroscopic studies of FeS_2 pyrite up to 675 K and 2100 MPa using a hydrothermal diamond anvil cell

XUEYIN YUAN AND HAIFEI ZHENG*

Key Laboratory of Orogenic Belts and Crustal Evolution, Ministry of Education, Peking University, Beijing 100871, China

[*Received 16 December 2013; Accepted 26 June 2014; Associate Editor: C. Geiger*]

ABSTRACT

Raman scattering experiments of natural FeS_2 pyrite were performed at simultaneous high-pressure and high-temperature conditions up to 675 K and 2100 MPa using a hydrothermal diamond anvil cell combined with micro-Raman spectroscopy. Four out of five Raman active modes [E_g, A_g, $T_g(1)$ and $T_g(3)$] were resolved at ambient conditions, the remaining $T_g(2)$ [~377 cm^{-1}] mode was weak and unresolved occurring ~2 cm^{-1} from the intense A_g [379 cm^{-1}] mode. The frequency shifts of the E_g [343 cm^{-1}] and A_g [379 cm^{-1}] modes were determined to be quadratic functions of pressure and temperature: $\nu_{343} = 343.35 - 0.0178 \times \Delta T - 8.4\text{E}{-6} \times (\Delta T)^2 + 0.00367 \times \Delta p - 3.7\text{E}{-7} \times (\Delta p)^2 + 1.0\text{E}{-6} \times \Delta T \times \Delta p$ and $\nu_{379} = 379.35 - 0.0295 \times \Delta T - 9.0\text{E}{-6} \times (\Delta T)^2 + 0.00460 \times \Delta p - 5.3\text{E}{-7} \times (\Delta p)^2 + 7.0\text{E}{-7} \times \Delta T \times \Delta p$. The positive pressure dependence of both modes indicates stress-induced contraction of S–S and Fe–S bonds, whereas the negative temperature dependence shows temperature-induced expansion of them. The Raman spectra of pyrite were used to derive its bulk modulus at high temperatures, thermal expansion coefficient at high pressures and anharmonic parameters at high-pressure and high-temperature conditions.

KEYWORDS: Raman spectra, pyrite, hydrothermal diamond anvil cell, high pressure and high temperature.

Introduction

FeS_2 pyrite is one of the most abundant sulfides and occurs in various geological conditions. The Fe–S system is of great importance in magmatic, hydrothermal and metamorphic processes and may have played an important role in the formation and evolution of the Earth's core (Ahrens and Jeanloz, 1987). It is, therefore, important to study the physical and chemical properties of pyrite at high-pressure and high-temperature conditions. Previous studies have shown that, possibly due to the low-spin 3d-orbital configuration of Fe^{2+}, pyrite appears to be widely stable up to 55 GPa and 320 GPa in static and shock compression experiments, respectively (Ahrens and Jeanloz, 1987; Merkel *et al.*, 2002; Kleppe and Jephcoat, 2004; Blanchard *et al.*, 2005).

The Raman vibrations of pyrite at ambient conditions have been published (Verble and Wallis, 1969; Ushioda, 1972; Vogt *et al.*, 1983; Mernagh and Trudu, 1993; Hope *et al.*, 2001) and several experiments have been carried out to study its vibrational properties at high pressures. Kleppe and Jephcoat (2004) observed positive pressure dependence for E_g, A_g, $T_g(1)$ and $T_g(3)$ modes of pyrite up to 55 GPa in diamond anvil cell experiments and determined Grüneisen parameters of 1.36, 1.40, 1.39 and 1.42 for these modes. Blanchard *et al.* (2005) calculated the vibrational frequencies of pyrite as a function of pressure and derived an average Grüneisen parameter of 1.30 for 0~50 GPa and 1.16 for 0~150 GPa. However, studies of the vibrational characterizations of pyrite

* E-mail: hfzheng@pku.edu.cn
DOI: 10.1180/minmag.2015.079.1.01

at high temperatures are absent, and the physical properties and anharmonicity of pyrite at high-pressure and high-temperature conditions are still unclear. In this paper we present an investigation of the Raman spectra of natural FeS_2 pyrite up to 675 K and 2100 MPa by using a hydrothermal diamond anvil cell (HDAC) combined with micro-Raman spectroscopy, with the objective of exploring the influence of applied pressure and temperature on the vibrational properties.

Experimental

A Bassett-type HDAC (Bassett *et al.*, 1993) was used to perform the experiments (Fig. 1*a*). Two opposed diamond anvils with 800 μm culets were mounted on tungsten-carbide seats and heated externally by Ni-Cr coils. The anvils were separated by a 250 μm thick rhenium gasket, with a 300 μm hole in the centre. Temperature was measured by a *K*-type thermocouple attached to the lower anvil, and was calibrated in advance by measuring the phase-transition temperatures of pure stearate, salicylate and sodium nitrate. The accuracy was ~±2 K and ±5 K at the temperatures below and above 500 K, respectively.

Raman spectra of samples were excited by a 514.5 nm Ar^+ laser and collected through a Renishaw-1000 confocal Raman system equipped with a 20× long focal-length objective (f = 35 mm). The spectral resolution of the system is ~2 cm^{-1}. All spectra were collected using a

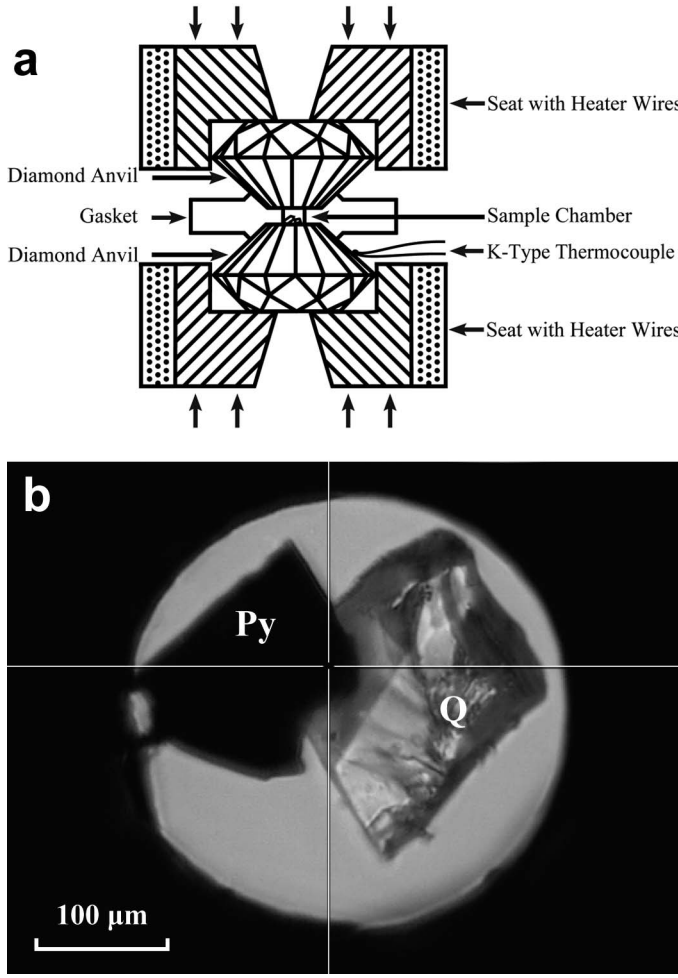

FIG. 1. (*a*) Schematic of the HDAC and (*b*) samples of pyrite (Py) and quartz (Q) in the chamber.

https://doi.org/10.1180/minmag.2015.079.1.01 Published online by Cambridge University Press

counting time of 60 s and an extended scanning mode from 100 to 800 cm^{-1}. Each collection was repeated five times. The spectral calibration of the system was carried out in advance with the 520.7 cm^{-1} line of the standard silicon wafer.

Crystals of natural pyrite and synthetic quartz were crushed into small pieces and two grains of pyrite (~100 μm × 70 μm) and quartz (~150 μm × 100 μm) were selected and placed in the chamber (Fig. 1*b*). Raman spectra of both minerals were first collected in Run 0, and then 20 wt.% NaCl solution was loaded as a pressure-transmitting medium before the chamber was sealed at ambient conditions. All measurements were made with the same pyrite and quartz samples, and six cycle runs with different starting pressures were carried out. During each cycle run, the temperature was increased from room to the target temperature with intervals of ~50 K, and a 3-min pause was made before collecting the Raman spectra to ensure the system was in equilibrium. The pressure was determined by the frequency shift of the 464 cm^{-1} peak of quartz at elevated pressure and temperature (p, T) from reference conditions ($p_{0.1\ MPa}$, $T_{273\ K}$) (Schmidt and Ziemann, 2000):

$$p\ (\text{MPa}) = 0.036079 \times [\nu(p, T) - \nu(p_{0.1\ MPa}, T)]^2 + 110.86 \times [\nu(p, T) - \nu(p_{0.1\ MPa}, T)]$$

$$\nu\ (p_{0.1\ MPa}, T)(cm^{-1}) = \nu(p_{0.1\ MPa}, T_{273\ K}) + 2.50136E{-}11 \times \Delta T^4 + 1.46454E{-}8 \times \Delta T^3 - 1.801E{-}5 \times \Delta T^2 - 0.01216 \times \Delta T \quad (1)$$

Where $\Delta T = T - T_{273\ K}$. The uncertainty of the pressure was ~±50 MPa based on the attainable accuracy for the Raman frequency of ~±0.4 cm^{-1}. The centre and the full width at half maximum (FWHM) of the peaks were then determined by fitting the spectra with the *PeakFit* V4.04 software package by Jandel Scientific.

Results

Pyrite crystallizes with cubic symmetry (space group *Pa*3) with lattice constant a = 5.418Å and sulfur fractional coordinate u = 0.385 (Brostigen and Kjekshus, 1969; Blanchard *et al.*, 2005). The irreducible representation for the vibrational matrix of pyrite is: $\Gamma = A_g + E_g + 3T_g + 2A_u + 2E_u + 6T_u$ (Lutz and Willich, 1974), among which only gerade modes are Raman active: the completely symmetric A_g mode corresponds to the in-phase stretching vibrations of the $(S_2)^{2-}$ dimer; in the doubly degenerate E_g mode the S atoms are displaced perpendicularly to the dimer axis and the triply degenerate T_g modes can be described by various librational and stretching vibrations or their combinations.

Raman spectra of pyrite and quartz

The transparent quartz was partly overlapped on the opaque pyrite in the chamber throughout the experiment (Fig. 1*b*), thus the spectra of both minerals could be acquired simultaneously by one scan when the laser was focused at the overlapping areas. Five peaks could be resolved in the spectrum collected at ambient conditions (Fig. 2): the intense 464 cm^{-1} peak belongs to the A_1 mode of quartz; the moderate 343 cm^{-1} and 379 cm^{-1} peaks represent E_g and A_g modes of pyrite; the weak 430 cm^{-1} peak is the $T_g(3)$ mode of pyrite, respectively, and the 352 cm^{-1} peak is an overlap of pyrite [$T_g(1)$, ~350 cm^{-1}] and quartz [A_1, ~353 cm^{-1}]. The remaining $T_g(2)$ mode of

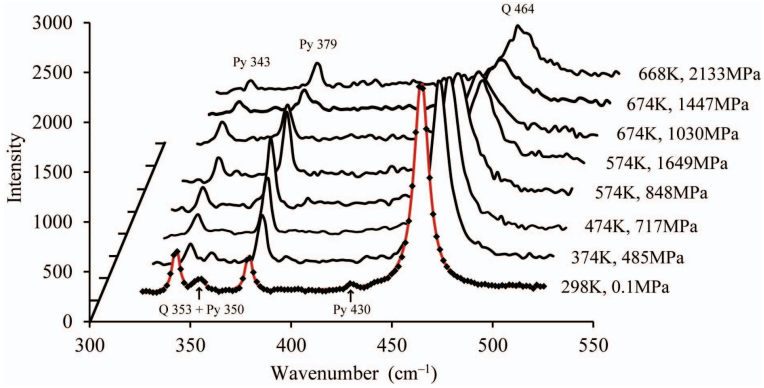

FIG. 2. Raman spectra of pyrite (Py) and quartz (Q) at ambient and high-*PT* conditions

https://doi.org/10.1180/minmag.2015.079.1.01 Published online by Cambridge University Press

pyrite is weak and occurs $\leqslant 2$ cm^{-1} away from the intense A_g peak (Vogt *et al.*, 1983); it could not be distinguished in our experiment.

As the T_g modes of pyrite were weak and not constantly observed at high temperatures (Fig. 2), only the 343 cm^{-1} and 379 cm^{-1} peaks of pyrite and the 464 cm^{-1} peak of quartz were fitted and are discussed in this study. The shape of these peaks was symmetric, similar to but slightly sharper than the Gaussian distribution. The Lorentz-Gauss cross-product function was used for peak fitting and the iterative computation was carried out until the squared correlation coefficients, r^2, were >0.99. The results are shown in Table 1. The uncertainty (1σ) for the centre of Raman peaks is better than ±0.4 cm^{-1} based on repeated data collection.

E_g and A_g mode Raman peaks at high pressures and high temperatures

The centre and FWHM for the E_g and A_g mode vibrations of pyrite at ambient conditions are 343.64 and 3.86 cm^{-1}, 379.66 and 3.93 cm^{-1}, respectively. All agree well with data published previously (Vogt *et al.*, 1983; Mernagh and Trudu, 1993; Kleppe and Jephcoat, 2004). We undertook several trials to fit the frequency shifts over the whole pressure and temperature ranges, and the following function gave the best results:

$$\nu(p,T) = \nu(p_0,T_0) + \Delta\nu(p,T) = \nu(p_0,T_0) + a \times \Delta T + b \times \Delta T^2 + c \times \Delta p + d \times \Delta p^2 + e \times \Delta T \times \Delta p \quad (2)$$

where $\nu(p_0,T_0)$ refers to the vibration frequency at 296 K and 0.1 MPa. The parameters a–e are achieved by fitting the data in Table 1 (T and p are replaced by ΔT and Δp) with *TableCurve 3D* V4.0 software package by SYSTAT Software Inc. and are shown in Table 2. The relationships between E_g and A_g vibration frequencies of pyrite, pressures and temperatures are illustrated in Fig. 3.

The FWHM for E_g and A_g modes of pyrite ranges mainly between 3.5 and 5.5 cm^{-1} and shows that the peak shape of both modes remains sharp and consistent at the experimental conditions. The FWHM increases slightly with temperature (Fig. 4), suggesting that the variance in the energy of both vibrations increases with temperature and results in peak broadening.

Discussion

The stability of FeS_2 pyrite over wide pressure ranges has been discussed in the literature (Ahrens and Jeanloz, 1987; Merkel *et al.*, 2002; Kleppe and Jephcoat, 2004). Our results show that both E_g and A_g modes of pyrite shift continuously to higher frequencies quasi-linearly with pressure at constant temperatures, or conversely, to lower frequencies with temperature at constant pressures. No indication of chemical reactions or structural phase transitions of pyrite were detected. The results further demonstrate that under hydrothermal conditions pyrite is stable at the experimental conditions.

Contribution of temperature and pressure to Raman vibrations

The $\partial\nu/\partial p$ slopes for the E_g and A_g modes of pyrite at room temperature are 0.00367−7.4E−7 $\times \Delta p$ cm^{-1}·MPa^{-1} and 0.00460 − 1.06E−6

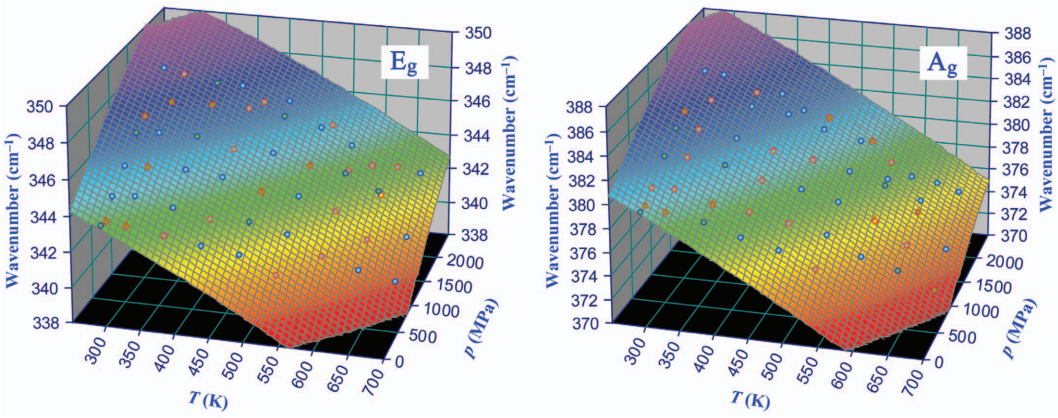

FIG. 3. Relationship between frequencies of the E_g (left) and A_g (right) modes, pressures and temperatures. Points below and above the fitted surface are coloured in red and blue, respectively.

https://doi.org/10.1180/minmag.2015.079.1.01 Published online by Cambridge University Press

TABLE 1. Raman spectra of pyrite collected at different pressure and temperature conditions.

Run	T (K)	Error[b]	P (MPa)	σ[c]	E_g (cm^{-1})	σ	FWHM	σ	A_g (cm^{-1})	σ	FWHM	σ
0.0[a]	296	1	0.1	2	343.64	0.17	3.86	0.31	379.66	0.13	3.93	0.31
1.1	296	1	115	4	343.59	0.04	4.20	0.33	379.70	0.06	4.28	0.35
1.2	323	1	165	3	343.24	0.05	4.09	0.11	379.15	0.06	4.24	0.15
1.3	374	1	235	2	342.77	0.10	4.29	0.56	378.30	0.12	4.33	0.32
1.4	423	1	325	9	342.20	0.24	4.27	0.37	377.01	0.12	4.50	0.24
1.5	474	2	421	14	341.60	0.12	4.35	0.17	375.87	0.15	4.84	0.35
1.6	524	2	483	16	340.50	0.18	4.73	0.44	374.33	0.11	5.09	0.20
2.1	296	1	275	13	344.54	0.13	4.34	0.98	380.54	0.08	3.52	0.33
2.2	323	1	385	11	344.40	0.07	4.35	0.53	380.23	0.07	3.97	0.26
2.3	374	1	485	9	343.69	0.12	5.07	0.51	378.85	0.11	4.50	0.29
2.4	423	1	595	8	342.95	0.16	4.98	0.35	378.07	0.04	3.94	0.14
2.5	474	2	717	6	342.68	0.12	4.76	0.31	376.94	0.11	3.64	0.21
2.6	524	2	817	14	341.87	0.27	4.81	0.51	375.80	0.08	4.14	0.20
2.7	574	2	848	12	340.75	0.18	4.77	0.53	374.18	0.07	4.13	0.25
2.8	624	2	920	11	340.01	0.23	4.64	0.48	372.92	0.14	4.72	0.52
3.1	298	1	591	8	345.48	0.10	4.25	0.29	382.07	0.07	4.37	0.33
3.2	323	1	727	14	345.13	0.20	4.21	0.39	381.60	0.18	4.51	0.54
3.3	374	1	846	3	344.86	0.10	4.41	0.44	380.74	0.06	5.00	0.39
3.4	423	1	954	12	344.39	0.27	4.81	0.49	379.37	0.15	4.92	0.32
3.5	474	2	1082	6	343.38	0.09	4.63	0.45	378.38	0.19	5.13	0.50
3.6	524	2	1190	13	343.08	0.22	4.91	0.43	377.17	0.13	4.96	0.40
3.7	574	2	1294	14	342.14	0.37	4.90	0.48	375.41	0.18	4.78	0.23
3.8	624	2	1237	76	340.86	0.15	4.97	0.49	373.89	0.23	4.95	0.25
4.1	298	1	894	3	346.60	0.06	4.15	0.17	383.26	0.06	4.21	0.28
4.2	323	1	1040	5	346.33	0.17	4.19	0.35	382.77	0.04	4.02	0.34
4.3	374	1	1174	8	345.96	0.12	4.24	0.37	381.82	0.15	4.04	0.27
4.4	423	1	1297	6	345.11	0.17	4.15	0.13	380.55	0.18	4.35	0.46
4.5	474	2	1441	6	344.70	0.15	4.06	0.12	379.48	0.09	3.89	0.12
4.6	524	2	1572	12	343.87	0.13	4.31	0.37	378.36	0.07	4.21	0.25
4.7	574	2	1649	9	343.43	0.10	3.92	0.37	377.13	0.08	4.22	0.15
4.8	624	2	1754	41	342.10	0.23	4.33	0.37	375.63	0.26	4.40	0.31
4.9	674	2	1030	14	339.20	0.25	4.83	0.53	371.21	0.15	5.00	0.35
5.1	296	1	1155	17	346.86	0.11	4.09	0.25	383.71	0.12	4.10	0.30
5.2	323	1	1413	9	347.17	0.17	4.12	0.35	383.94	0.09	4.12	0.17
5.3	374	1	1592	13	346.75	0.04	3.92	0.34	383.11	0.08	4.14	0.24
5.4	423	1	1740	13	346.41	0.06	4.18	0.44	382.12	0.12	4.23	0.29
5.5	474	2	1823	23	345.89	0.17	4.36	0.55	380.81	0.04	4.34	0.26
5.6	524	2	1953	16	345.09	0.11	4.22	0.41	379.57	0.25	4.72	0.37
5.7	574	2	1726	33	343.37	0.22	4.84	0.49	377.34	0.17	4.89	0.48
5.8	624	2	1660	38	342.52	0.05	4.63	0.60	375.03	0.28	4.99	0.38
5.9	674	2	1447	28	340.64	0.19	4.84	0.49	372.99	0.03	5.17	0.50
6.1	298	1	1662	3	348.51	0.20	4.65	0.39	385.51	0.10	4.06	0.35
6.2	324	1	1738	5	348.02	0.18	4.06	0.41	385.06	0.06	3.56	0.19
6.3	373	1	1773	12	347.59	0.24	4.05	0.36	383.61	0.13	3.91	0.22
6.4	405	1	1929	9	347.23	0.15	4.31	0.35	383.14	0.26	4.01	0.24
6.5	439	1	1884	8	346.48	0.13	4.12	0.39	382.00	0.19	4.34	0.44
6.6	472	2	2017	10	346.32	0.36	4.18	0.56	381.05	0.25	4.43	0.29
6.7	537	2	2069	15	345.05	0.19	4.54	0.35	379.22	0.20	4.35	0.24
6.8	570	2	1964	16	344.23	0.09	4.21	0.68	377.91	0.20	4.28	0.47
6.9	602	2	1930	20	343.27	0.16	4.65	0.40	377.00	0.11	4.62	0.34
6.10	636	2	2060	12	342.96	0.10	4.32	0.76	376.13	0.11	4.56	0.53
6.11	668	2	2133	8	342.52	0.13	4.43	0.54	375.27	0.15	4.54	0.29

Note: [a] – data collected in Run 0 at ambient conditions; [b] – precision of the temperature, which is less than the accuracy; [c] – pressure uncertainty calculated from the attainable precision of the 464 cm^{-1} line of quartz.

https://doi.org/10.1180/minmag.2015.079.1.01 Published online by Cambridge University Press

TABLE 2. Results of fitting the Raman spectra with function 2.

Modes	$\nu(p_0, T_0)$	a	$b \times 10^{-6}$	c	$d \times 10^{-7}$	$e \times 10^{-6}$	R^2
E_g	343.35(9)	−0.0178(8)	−8.4(21)	0.00367(20)	−3.7(10)	1.0(5)	0.9951
A_g	379.35(9)	−0.0295(7)	−9.0(20)	0.00460(18)	−5.3(9)	0.7(5)	0.9982

$\times \Delta p$ $cm^{-1}{\cdot}MPa^{-1}$, respectively. As it has been confirmed that the E_g and A_g modes of pyrite are governed mainly by the Fe−S and S−S force constant (Sourisseau *et al.*, 1991; Lutz and Zwinscher, 1996), the positive pressure dependence of both modes shows pressure-induced contractions for the Fe−S and S−S bonds of pyrite under compression, which agrees well with previous studies (Fujii *et al.*, 1986; Sourisseau *et al.*, 1991; Merkel *et al.*, 2002; Kleppe and Jephcoat, 2004; Blanchard *et al.*, 2005). The $\partial\nu/\partial p$ slopes at low pressures (e.g. <1 GPa) are significantly higher than those reported by Kleppe and Jephcoat (2004). However, these slopes show good consistency at high pressures (e.g. >1.5 GPa) due to the larger absolute $\partial^2\nu/\partial p^2$ values in the present results, suggesting that the Fe−S and S−S bonds of pyrite are more sensitive to stress changes at low pressures than reported previously.

The $\partial\nu/\partial T$ slopes for E_g and A_g modes at ambient pressure are $-0.0178-1.68E-5\times\Delta T$ $cm^{-1}{\cdot}K^{-1}$ and $-0.0295-1.80E-5\times\Delta T$ $cm^{-1}{\cdot}K^{-1}$. The negative temperature dependence of both modes indicates temperature-induced expansion for the Fe−S and S−S bonds of pyrite. The negative $\partial^2\nu/\partial T^2$s imply larger $\partial\nu/\partial T$ slopes and stronger thermal expansibility of pyrite at high temperatures. This result is in good agreement with the conclusions of other studies (Press, 1949; Chrystall, 1965; Bindloss, 1971; Ellmer and Höpfner, 1997).

Our results show that pressure and temperature also have a related impact on the vibrational characteristics of pyrite. Compared with the effects of pressure and temperature on the vibrations of pyrite at ambient conditions, the positive $\partial^2\nu/\partial p\partial T$ terms suggest greater influence of pressure on both vibrations or larger compressibility for S−S and Fe−S bonds at high temperatures; or conversely, weaker influence of temperature on vibrations, or smaller expansibility of S−S and Fe−S bonds at high pressures. The related impacts of pressure and temperature on the physical properties of pyrite will be further discussed in the following sections.

Isothermal Grüneisen parameter and bulk modulus

The isothermal Grüneisen parameter (γ_{iT}) is used widely to describe the mineral property whereby the vibrational frequencies of crystals increase proportionally with compression of volume. In

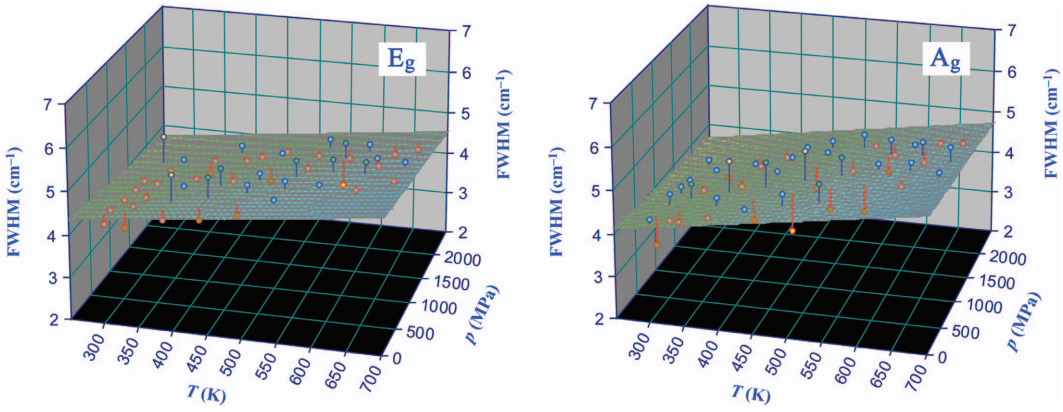

FIG. 4. Relationship between the FWHM of the E_g (left) and A_g (right) modes, pressures and temperatures.

https://doi.org/10.1180/minmag.2015.079.1.01 Published online by Cambridge University Press

this study, γ_{iT} for the E_g and A_g modes of pyrite have been found to be 1.25 and 1.38 at ambient temperature by fitting the frequency shifts with the following functional dependence on pressure, which is similar to the Murnaghan equation of state (Murnaghan, 1937):

$$\nu = \nu_0 \times \left[1 + p \times \frac{B_0'}{B_0}\right]^{(\gamma_{iT}/B_0')} \quad (3)$$

where bulk modulus, B_0 = 138.9GPa at ambient pressure, and its pressure derivative, B_0'= 6.0, are taken from Whitaker *et al.* (2010). Our results agree well with 1.36 and 1.40 presented by Kleppe and Jephcoat (2004).

The bulk modulus of a hard solid could be derived from Raman spectra if the isothermal Grüneisen parameter is known or well constrained (Datchi and Canny, 2004; Datchi *et al.*, 2007). By reasonably assuming that γ_{iT} for the E_g and A_g modes of pyrite is independent of temperature, and that the variation of B_0' with temperature is negligible in the range spanned by the experiment, the $B_0(T)$ of pyrite and its temperature derivative could be extracted from the Raman spectra collected at high-pressure and high-temperature conditions, based on the Raman frequency as a function of pressure at high temperatures:

$$\nu(p, T) = \nu(0, T) \times \left[1 + p \times \frac{B_0'}{B_0(T)}\right]^{(\gamma_{iT}/B_0')} \quad (4)$$

By fitting the data of the E_g and A_g vibrations with pressure at specific temperatures, and assuming that the contributions to $B_0(T)$ from S−S and Fe−S bonds are equal, the $B_0(T)$ of pyrite and its temperature derivative are obtained and are shown in Fig. 5. The modulus of pyrite is seen to decrease with temperature, indicating that the mineral is more easily compressed at high temperatures. By comparison, the temperature derivative of the modulus of pyrite, as measured by ultrasonic methods by Benbattouche *et al.* (1989), is about −0.01 GPa·K^{-1} from 100 to 300 K.

Isobaric Grüneisen parameter and thermal expansion coefficient

It has been demonstrated extensively that vibrational frequencies of solids shift proportionally with thermal expansion of the volume and could be described by isobaric Grüneisen parameters (γ_{ip}) (Gillet *et al.*, 1989, 1990; Lucazeau, 2003). In the present study, the γ_{ip} for E_g and A_g mode vibrations of pyrite obtained are 1.88 and 2.65 at ambient pressure by fitting the frequency shifts with the following functional dependence on temperature:

$$\nu = \nu_0 \times \mathrm{Exp}[\gamma_{ip} \times (\alpha \times \Delta T + 1/2 \times \alpha' \times \Delta T^2)] \quad (5)$$

where the volumetric thermal expansion coefficient of pyrite, $\alpha = 2.54 \times 10^{-5}$ K^{-1} at 296 K and its temperature derivative, $\alpha' = 4.3873 \times 10^{-8}$, are taken from Fei (1995).

In order to investigate the effect of pressure on the thermal expansion coefficient of pyrite, we assume that the isobaric Grüneisen parameters (γ_{ip}) and the temperature derivative of thermal expansion coefficient (α') are independent of

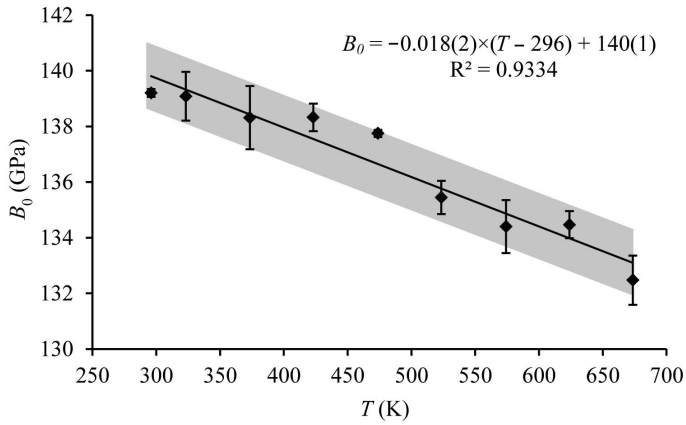

FIG. 5. Bulk modulus of pyrite and its temperature dependence.

https://doi.org/10.1180/minmag.2015.079.1.01 Published online by Cambridge University Press

pressure in the range covered by the experiment, and that equation 5 can be generalized at high pressures as:

$$\nu(p,T) = \nu(p,T_0) \times \mathrm{Exp}\{\gamma_{ip} \times [\alpha(p) \times \Delta T + 1/2 \times \alpha' \times \Delta T^2]\} \quad (6)$$

with

$$\nu(p,T_0) = \nu(p,T) - a \times \Delta T - b \times \Delta T^2$$

where a and b are determined by function 2 and are listed in Table 2. By fitting the E_g and A_g mode vibrations with temperature at specific pressures and assuming that contributions to $\alpha(p)$ from S–S and Fe–S bonds are equal, the $\alpha(p)$ of pyrite and its pressure derivative are obtained and displayed in Fig. 6. We can see that the thermal expansion coefficient of pyrite decreases with pressure, suggesting that the expansibility of the mineral becomes less at high pressures.

Anharmonicity

It can be seen that at ambient conditions, the γ_{ip} for E_g and A_g modes of pyrite (1.88 and 2.65) are significantly larger than the γ_{iT} (1.25 and 1.38), indicating that the frequency shifts of both modes are contributed not only from volume changes of the mineral (either by stress-induced compression or by temperature-induced expansion), but also arise from higher-order anharmonic interactions. Gillet *et al.* (1990) used an anharmonic parameter, a_i, to describe the crystal anharmonicity, which is expressed as a shift in frequency due to temperature at constant volume:

$$a_i = (\partial \ln \nu_i / \partial T)_V = \alpha \times (\gamma_{iT} - \gamma_{ip}) \quad (7)$$

where α, γ_{iT} and γ_{ip} refer to the volumetric thermal expansion coefficient, isothermal and isobaric Grüneisen parameters, respectively. In principle, for a quasi-harmonic approximation where bands behave harmonically, $\gamma_{iT} = \gamma_{ip}$ and $a_i = 0$; while in an anharmonic case where frequency shifts are at the same time contributed from anharmonic interactions, the γ_{iT} and γ_{ip} are not equal and $a_i \neq 0$ (Gillet *et al.*, 1990; Lucazeau, 2003). In the present study, the anharmonic parameters of E_g and A_g modes decrease from $-1.59 \times 10^{-5} K^{-1}$ and $-3.21 \times 10^{-5} K^{-1}$ at ambient conditions to -2.46×10^{-5} K^{-1} and -4.95×10^{-5} K^{-1} at 675 K and 2100 MPa. The intrinsic anharmonicity of pyrite contributes significantly to its optical vibrations, and the S–S related vibration is more anharmonic.

Due to the anharmonicity of solids, the values of specific heat at constant volume measured from experiments are commonly greater than those calculated using quasi-harmonic approximation when the temperature is higher than Debye temperatures. An anharmonic parameter has been used extensively to provide excellent corrections for these deviations (Gillet *et al.*, 1990; Gillet *et al.*, 2000; Fujimori *et al.*, 2002; Rao *et al.*, 2013). According to a modification of Kieffer's model with an anharmonic parameter by Gillet *et al.* (1990), the specific heat is given by:

$$C_V^{\mathrm{anh}} = 3nR \times \Sigma[C_{Vi}(1 - 2 \times a_i \times T)] \quad (8)$$

where C_V^{anh} is the specific heat in anharmonic cases, C_{Vi} and a_i refer to the harmonic contribution to C_V and the anharmonic parameter of the *ith* continuum. Although our results do not

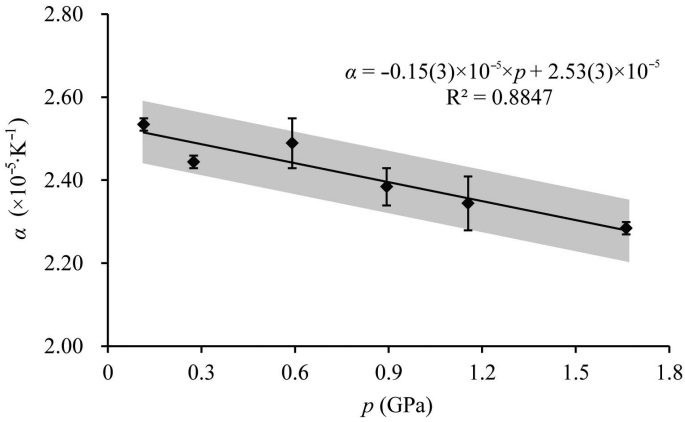

FIG. 6. Thermal expansion coefficient of pyrite and its pressure dependence.

https://doi.org/10.1180/minmag.2015.079.1.01 Published online by Cambridge University Press

give the exact C_V^{anh} of pyrite at different temperatures, it suggests that the contributions to C_V of E_g and A_g mode vibrations are 3.3% and 6.8% higher than those calculated using a quasi-harmonic approximation at 675 K and 2100 MPa. The result provides some insights into the thermodynamic properties of pyrite contributed from the anharmonicity of its optical vibrations at high pressures and high temperatures.

Acknowledgements

This work was supported by Natural Science Foundation of China (Nos. 40873047 and 41373057). The authors are grateful to three anonymous reviewers for their valuable suggestions and comments.

References

Ahrens, T.J. and Jeanloz, R. (1987) Pyrite: Shock compression, isentropic release, and composition of the Earth's core. *Journal of Geophysical Research: Solid Earth (1978–2012)*, **92**, 10363–10375.

Bassett, W., Shen, A., Bucknum, M. and Chou, I.M. (1993) A new diamond anvil cell for hydrothermal studies to 2.5 GPa and from −190 to 1200ºC. *Review of Scientific Instruments*, **64**, 2340–2345.

Benbattouche, N., Saunders, G., Lambson, E. and Honle, W. (1989) The dependences of the elastic stiffness moduli and the poisson ratio of natural iron pyrites FeS_2 upon pressure and temperature. *Journal of Physics D: Applied Physics*, **22**, 670.

Bindloss, W. (1971) Anomalous exchangestriction in ferromagnetic pyrite and chromium chalcogenide spinel compounds. *Journal of Applied Physics*, **42**, 1474.

Blanchard, M., Alfredsson, M., Brodholt, J., Price, G.D., Wright, K. and Catlow, C.R.A. (2005) Electronic structure study of the high-pressure vibrational spectrum of FeS_2 pyrite. *The Journal of Physical Chemistry B*, **109**, 22067–22073.

Brostigen, G. and Kjekshus, A. (1969) Redetermined crystal structure of FeS_2-pyrite. *Acta Chemica Scandinavica*, **23**, 2186–2188.

Chrystall, R. (1965) Thermal expansion of iron pyrites. *Transactions of the Faraday Society*, **61**, 1811–1815.

Datchi, F. and Canny, B. (2004) Raman spectrum of cubic boron nitride at high pressure and temperature. *Physical Review B*, **69**, 144106.

Datchi, F., Dewaele, A., Le Godec, Y. and Loubeyre, P. (2007) Equation of state of cubic boron nitride at high pressures and temperatures. *Physical Review B*, **75**, 214104.

Ellmer, K. and Höpfner, C. (1997) On the stoichiometry of the semiconductor pyrite (FeS_2). *Philosophical Magazine A*, **75**, 1129–1151.

Fei, Y. (1995) Thermal expansion. Pp. 29–44 in: *Mineral Physics and Crystallography: a Handbook of Physical Constants* (T.J. Ahrens, editor). AGU Reference Shelf, Vol. **2**. American Geophysical Union, Washington, DC..

Fujii, T., Yoshida, A., Tanaka, K., Marumo, F. and Noda, Y. (1986) High pressure compressibilities of pyrite and cattierite. *Mineralogical Journal*, **13**, 202–211.

Fujimori, H., Komatsu, H., Ioku, K., Goto, S. and Yoshimura, M. (2002) Anharmonic lattice mode of Ca_2SiO_4: Ultraviolet laser Raman spectroscopy at high temperatures. *Physical Review B*, **66**, 064306.

Gillet, P., Guyot, F. and Malezieux, J.-M. (1989) High-pressure, high-temperature Raman spectroscopy of Ca_2GeO_4(olivine form): Some insights on anharmonicity. *Physics of the Earth and Planetary Interiors*, **58**, 141–154.

Gillet, P., Le Cléac'h, A. and Madon, M. (1990) High-temperature raman spectroscopy of SiO_2 and GeO_2 polymorphs: Anharmonicity and thermodynamic properties at high-temperatures. *Journal of Geophysical Research: Solid Earth*, **95**, 21635–21655.

Gillet, P., Daniel, I., Guyot, F., Matas, J. and Chervin, J.-C. (2000) A thermodynamic model for $MgSiO_3$-perovskite derived from pressure, temperature and volume dependence of the Raman mode frequencies. *Physics of the Earth and Planetary Interiors*, **117**, 361–384.

Hope, G.A., Woods, R. and Munce, C.G. (2001) Raman microprobe mineral identification. *Minerals Engineering*, **14**, 1565–1577.

Kleppe, A. and Jephcoat, A. (2004) High-pressure Raman spectroscopic studies of FeS_2 pyrite. *Mineralogical Magazine*, **68**, 433–441.

Lucazeau, G. (2003) Effect of pressure and temperature on Raman spectra of solids: Anharmonicity. *Journal of Raman Spectroscopy*, **34**, 478–496.

Lutz, H. and Willich, P. (1974) Lattice vibration spectra. IX. Pyrite structure. FIR spectra and normal coordinate analysis of MnS_2, FeS_2, and NiS_2. *Zeitschrift für Anorganische und Allgemeine Chemie*, **405**, 176–182.

Lutz, H. and Zwinscher, J. (1996) Lattice dynamics of pyrite FeS_2 – polarizable-ion model. *Physics and Chemistry of Minerals*, **23**, 497–502.

Merkel, S., Jephcoat, A., Shu, J., Mao, H.-K., Gillet, P. and Hemley, R. (2002) Equation of state, elasticity, and shear strength of pyrite under high pressure. *Physics and Chemistry of Minerals*, **29**, 1–9.

Mernagh, T.P. and Trudu, A.G. (1993) A laser Raman microprobe study of some geologically important

https://doi.org/10.1180/minmag.2015.079.1.01 Published online by Cambridge University Press

sulphide minerals. *Chemical Geology*, **103**, 113–127.

Murnaghan, F.D. (1937) Finite deformations of an elastic solid. *American Journal of Mathematics*, **59**, 235–260.

Press, D. (1949) Thermal expansion of fluorspar and iron pyrite. *Proceedings Mathematical Sciences*, **30**, 284–294.

Rao, R., Salke, N.P. and Garg, A.B. (2013) Raman spectroscopic study of phase stability and anharmonicity in $Bi_{12}TiO_{20}$. *Materials Chemistry and Physics*.

Schmidt, C. and Ziemann, M.A. (2000) In-situ Raman spectroscopy of quartz: A pressure sensor for hydrothermal diamond-anvil cell experiments at elevated temperatures. *American Mineralogist*, **85**, 1725–1734.

Sourisseau, C., Cavagnat, R. and Fouassier, M. (1991) The vibrational properties and valence force fields of FeS_2, RuS_2 pyrites and FeS_2 marcasite. *Journal of Physics and Chemistry of Solids*, **52**, 537–544.

Ushioda, S. (1972) Raman scattering from phonons in iron pyrite (FeS_2). *Solid State Communications*, **10**, 307–310.

Verble, J. and Wallis, R. (1969) Infrared studies of lattice vibrations in iron pyrite. *Physical Review*, **182**, 783.

Vogt, H., Chattopadhyay, T. and Stolz, H. (1983) Complete first-order Raman spectra of the pyrite structure compounds FeS_2, MnS_2 and SiP_2. *Journal of Physics and Chemistry of Solids*, **44**, 869–873.

Whitaker, M.L., Liu, W., Wang, L. and Li, B. (2010) Acoustic velocities and elastic properties of pyrite (FeS_2) to 9.6 GPa. *Journal of Earth Science*, **21**, 792–800.

https://doi.org/10.1180/minmag.2015.079.1.01 Published online by Cambridge University Press